

Effects of modulation p doping in InAs quantum dot lasers on silicon

Zeyu Zhang, Daehwan Jung, Justin C. Norman, Pari Patel, Weng W. Chow, and John E. Bowers

Citation: *Appl. Phys. Lett.* **113**, 061105 (2018); doi: 10.1063/1.5040792

View online: <https://doi.org/10.1063/1.5040792>

View Table of Contents: <http://aip.scitation.org/toc/apl/113/6>

Published by the [American Institute of Physics](#)

Articles you may be interested in

[Monolithic 9 GHz passively mode locked quantum dot lasers directly grown on on-axis \(001\) Si](#)
Applied Physics Letters **113**, 041108 (2018); 10.1063/1.5043200

[Semiconductor quantum dot lasers epitaxially grown on silicon with low linewidth enhancement factor](#)
Applied Physics Letters **112**, 251111 (2018); 10.1063/1.5025879

[Impact of threading dislocation density on the lifetime of InAs quantum dot lasers on Si](#)
Applied Physics Letters **112**, 153507 (2018); 10.1063/1.5026147

[Perspective: The future of quantum dot photonic integrated circuits](#)
APL Photonics **3**, 030901 (2018); 10.1063/1.5021345

[InAs QDs on \(111\)-faceted Si \(001\) hollow substrates with strong emission at 1300 nm and 1550 nm](#)
Applied Physics Letters **113**, 053107 (2018); 10.1063/1.5043169

[Low dissipation spectral filtering using a field-effect tunable III–V hybrid metasurface](#)
Applied Physics Letters **113**, 061108 (2018); 10.1063/1.5042662

AIP | Conference Proceedings

Get **30% off** all
print proceedings!

Enter Promotion Code **PDF30** at checkout



Effects of modulation p doping in InAs quantum dot lasers on silicon

Zeyu Zhang,^{1,a)} Daehwan Jung,^{2,3} Justin C. Norman,^{2,3} Pari Patel,¹ Weng W. Chow,⁴
 and John E. Bowers^{1,2,3}

¹Electrical and Computer Engineering Department, University of California Santa Barbara, Santa Barbara, California 93106, USA

²Material Department, University of California Santa Barbara, Santa Barbara, California 93106, USA

³Institute for Energy Efficiency, University of California Santa Barbara, 2314 Phelps Hall, Santa Barbara, California 93106, USA

⁴Sandia National Laboratories, Albuquerque, New Mexico 87185-1086, USA

(Received 21 May 2018; accepted 24 July 2018; published online 7 August 2018)

We investigate, both experimentally and theoretically, the gain characteristics of modulation p -doped $1.3\ \mu\text{m}$ quantum dot lasers epitaxially grown on silicon. Gain spectra and transparency points are measured for structurally identical lasers with varying levels of p doping in the active region. A many-body model is employed to facilitate understanding of the material gain characteristics. It has been found that appropriate p doping greatly reduces transparency and improves differential gain. It is also found that the improvements saturate with excessive doping because of the increase in nonradiative carrier recombination. *Published by AIP Publishing.*

<https://doi.org/10.1063/1.5040792>

Realizing the epitaxial growth of semiconductor lasers on silicon has been regarded as an important milestone for integrating light sources in silicon photonics.¹ However, the large lattice mismatch between silicon (Si) and the grown III-V material naturally introduces threading dislocations (TDs) to the laser epitaxy. Quantum dot (QD) lasers, due to the three-dimensional confinement of carriers, have been experimentally proven to be far less sensitive to the damaging effects of TDs as compared to quantum well (QW) lasers.² GaAs buffer layers employing strained-layer superlattices and thermal cyclic annealing can further prevent TDs from propagating into the active region, reducing the dislocation density from $\sim 1 \times 10^8\ \text{cm}^{-2}$ to $7 \times 10^6\ \text{cm}^{-2}$.²⁻⁴ Such reduction in defect density results in drastic improvement in device lifetime from $\sim 4.5 \times 10^3\ \text{h}$ ⁵ to extrapolated lifetimes of $\sim 10 \times 10^6\ \text{h}$ ⁶ when aged at $35\ ^\circ\text{C}$.

As the material quality of QD lasers on Si approaches that of lasers grown on native substrates, it is now of increasing interest to realize devices with specialized functionality (*e.g.*, single-mode laser,⁷ mode-locked laser,⁸ and narrow linewidth laser) within the monolithic integration platform. For a directly modulated single-mode laser in a communication link, the power budget and bandwidth requirement necessitate low threshold and high relaxation oscillation frequency; a mode-locked laser requires a large extinction ratio in the saturation energy between the gain region and the saturable absorber; a narrow linewidth laser, by definition, needs a small linewidth enhancement factor. These device metrics, although generated by different applications, can all be translated to the demands for lower transparency current, higher material gain, and higher differential gain.⁹⁻¹¹ In QW lasers, such goals are accomplished by compressively straining the QW layers to increase the curvature in the valence band.⁹ Engineering the strain profile in the QD active region to optimize gain performance is not practical because strain

also greatly affects the lasing wavelength and the formation process of the QDs.¹² Instead, p -type doping is introduced in the GaAs spacer layers between QD layers to lower the quasi-Fermi level in the valence band, thereby providing lower transparency and larger material gain.¹³ Previous effort has demonstrated that p doping indeed improves overall gain characteristics of QD lasers.^{14,15} The impact of p doping on the laser modulation response has been predicted and verified.¹⁶⁻¹⁸ p doping has also been proved to facilitate ground-state (GS) lasing in short-cavity lasers due to improvement in the GS gain and hole-to-electron capture rate ratio.^{15,19} However, the effect of p doping on the gain performance in the QD active region has not been studied by a first-principles gain model. Such a model would require careful treatment of the many-body effects, which are crucial to the calculation of the carrier scattering rate and, for the same reason, homogeneous linewidth of the gain spectrum.²⁰ The elimination of free or fitting parameters from the calculation grants more accurate assessment of the gain performance in QD lasers.

In the present work, we demonstrate the direct measurement of material gain and transparency current in QD laser active regions with varying levels of modulation p doping. A many-body gain model with scattering treated at the level of quantum kinetic equations is employed to calculate the gain spectra under the same scenarios. Inhomogeneous broadening and carrier recombination coefficients can then be determined by comparing the experimental and calculated gain, without taking assumptions of other fitting parameters. We show that appropriate p doping drastically improves the gain performance by lowering transparency and increasing differential gain. As the p doping is further increased, the state-filling effect, increased carrier scattering rate, and increased nonradiative recombination will start to slow down the improvements.

Three batches of the laser with unintentionally doped (UID), $5 \times 10^{17}\ \text{cm}^{-3}$ and $1 \times 10^{18}\ \text{cm}^{-3}$ p -type dopant

^{a)}Email: z_zhang@umail.ucsb.edu

concentrations in the active region are grown and fabricated. The lasers are otherwise identical. The growth conditions and device fabrication steps have been reported in detail elsewhere.⁴ The *p*-type Beryllium dopants are introduced in a 10-nm thick GaAs region within the 40 nm spacer layer below each dot-in-a-well (DWELL) layer. Given the dot density of $\sim 5 \times 10^{10} \text{ cm}^{-2}$, the selected doping concentrations correspond to, on average, 0, 10, and 20 extra holes per QD.

After laser sample preparation, amplified spontaneous emission (ASE) spectra are measured at different current injection levels for ridge lasers of dimension $3.5 \mu\text{m} \times 1500 \mu\text{m}$. The mode-sum method²¹ is then employed to extract the net modal gain from the ASE spectra. Afterward, transparency current is directly measured for different wavelengths using a modulated external probe laser, utilizing the optical detection property of the laser medium.²² The combination of the net modal gain and transparency measurement allows the extraction of material gain in the laser active regions under investigation.²³ The experimental setup has been described in detail in a previous report.⁴

To calculate the laser gain, we first solve the equation of motion for the electron-hole polarization $p_{\alpha\beta}$

$$\frac{dp_{\alpha\beta}}{dt} = i\omega_{\alpha\beta}p_{\alpha\beta} - i\Omega_{\alpha\beta}(n_{\alpha}^e + n_{\beta}^h - 1) + S_{\alpha\beta}^{c-p} + S_{\alpha\beta}^{c-c}, \quad (1)$$

where $\omega_{\alpha\beta}$ and $p_{\alpha\beta}$ are the renormalized transition and Rabi frequencies, and n_{α} and n_{β} are the electron and hole populations in states α and β . Dephasing contributions from carrier-phonon and carrier-carrier scattering are given by $S_{\alpha\beta}^{c-p}$ and $S_{\alpha\beta}^{c-c}$, respectively. Details for their evaluation are described in the literature.²⁴ The input to the calculations is the electron and hole energy levels, as well as the optical dipole matrix elements, computed using a Schrödinger-Poisson solver.²⁵ The steady-state solution of (1) gives the material gain according to

$$G_M(\omega) = -\frac{\omega}{\varepsilon_0 n c V E(\omega)} \text{Im} \left(\sum_{\alpha\beta} \mu_{\alpha\beta} p_{\alpha\beta} \right), \quad (2)$$

where ε_0 and c are the permittivity and speed of light in vacuum, $\mu_{\alpha\beta}$ is the dipole matrix element, n is the background refractive index, $E(\omega)$ is the laser electric field amplitude, ω is its frequency, V is the DWELL volume, and the summation is overall QD and QW states. Note that material gain should be approximately proportional to the difference between the Fermi function in the conduction and valence bands ($G_M = G_{\text{max}}(f_c - f_v)$).⁹ Consequently, it is instructive to examine the degree of population inversion at different doping levels. The average ground-state population as a function of doping density and carrier density is shown in Fig. 1(a). Evidently, *p* doping greatly increases the occupation probability of holes in the ground state at the valence band, resulting in direct enhancement of population inversion. It can also be expected that the state-filling effect would prevent the additional *p* doping from creating the same amount of population inversion. Indeed, the increase in the ground-state hole population from the doping level of $5 \times 10^{17} \text{ cm}^{-3}$ to $1 \times 10^{18} \text{ cm}^{-3}$ is smaller than that from $1 \times 10^{17} \text{ cm}^{-3}$ to $3 \times 10^{17} \text{ cm}^{-3}$. Many-body effects, enhanced

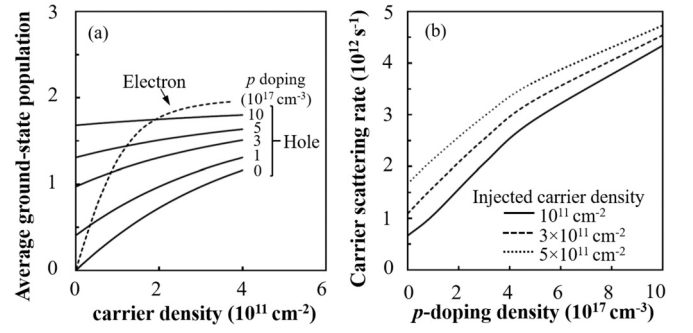


FIG. 1. (a) Average ground state electron and hole populations versus injected carrier density for different *p*-doping densities. (b) Carrier scattering rate versus *p*-doping density for different injected carrier densities. Both results are used in the gain spectrum calculations for a 7 nm $\text{In}_{0.15}\text{Ga}_{0.85}\text{As}$ QW layer embedding a density of $5 \times 10^{10} \text{ cm}^{-2}$ InAs QDs.

by the local confinement of the carrier, greatly influence the material gain in homogeneous QD population. As indicated in Fig. 1(b), the introduction of a *p*-doping density of $1 \times 10^{18} \text{ cm}^{-3}$ increases the carrier scattering rate by roughly eight times compared to the UID case. This will result in a broader homogeneous linewidth and lower peak gain, partially negating the benefit of enhanced population inversion created by *p* doping.

In the presence of inhomogeneous broadening due to QD size fluctuations, we performed a statistical average over a range of band-gap energies ε :

$$G_M^{\text{inh}}(\omega) = \int_{-\infty}^{\infty} d\varepsilon \frac{1}{\sqrt{2\pi}\Delta_{\text{inh}}} \exp \left[-\left(\frac{\varepsilon - \varepsilon_g}{\sqrt{2}\Delta_{\text{inh}}} \right)^2 \right] G_M(\omega, \varepsilon), \quad (3)$$

where ε_g is the InAs band-gap energy, and we assume a weighting described by a normal distribution characterized by an inhomogeneous broadening width Δ_{inh} . $G_M(\omega, \varepsilon)$ is the homogeneous gain in (2), with an added parameter ε to indicate that the homogeneously broadened quantities are computed for a precise electronic structure. The material gain spectra at different *p*-doping levels are shown in Fig. 2(a). It

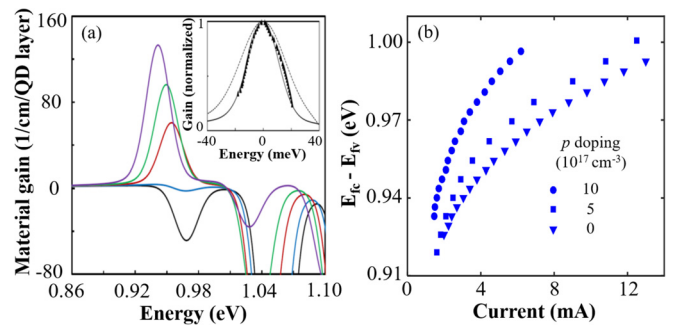


FIG. 2. (a) Computed room temperature material gain spectra for an injected carrier density of 10^{11} cm^{-2} and 10 meV inhomogeneous broadening. The spectra are for undoped (back curve) and *p*-doping density (with increasing ground-state gain) $1 \times 10^{17} \text{ cm}^{-3}$, $3 \times 10^{17} \text{ cm}^{-3}$, $5 \times 10^{17} \text{ cm}^{-3}$, and $1 \times 10^{18} \text{ cm}^{-3}$. In the inset, the data points are measured for a UID QD laser at 13 mA. The curves are calculated for 10 meV and 15 meV inhomogeneous broadening (solid and dotted curves, respectively). The injected carrier density is $1.7 \times 10^{11} \text{ cm}^{-2}$. All other parameters are the same as in Fig. 1. (b) Measurement results of transparency points at different *p* doping levels. The ordinate is labeled as quasi-Fermi level separation since it equals the photon energy at transparency.

can be clearly seen that, at the same carrier density and Δ_{inh} , higher material gain can be achieved with increased p -doping density. A more subtle observation, yet consistent with the discussions of the state-filling effect and carrier scattering, can be made on the decline of the enhancement in material gain with the same amount of additional p doping. A direct consequence of increased gain at higher p doping is the reduced current (carrier density) when the active region reaches transparency [$G_{\text{M}}^{\text{inh}}(\omega) = 0$]. This is experimentally verified by direct transparency measurement results shown in Fig. 2(b). Comparing the experimentally measured gain spectra and the ones calculated from theory permits estimation of Δ_{inh} , which is hard to quantitatively determine experimentally due to uncertainty of the homogeneous linewidth. Such an extraction is shown in the inset of Fig. 2(a), in which the measured gain spectrum closely matches the calculated gain spectrum with $\Delta_{\text{inh}} = 10$ meV. Extraction at other doping levels generates very similar results. Another way to determine Δ_{inh} is through its relationship with the spectral width of the photoluminescence (PL) measurement. Our samples show a typical PL full-width at half-maximum (FWHM) of 28 meV, which, without surprise, corresponds to Δ_{inh} of 10 meV.²⁰ It is worth noting that a previous effort on applying the same extraction technique to QD lasers on silicon reports $\Delta_{\text{inh}} \approx 20$ meV.²⁶ The 50% drop in Δ_{inh} showcases the improvement in material quality achieved in the past few years.

Experimentally, gain spectra are measured at various current injection levels up to threshold, while the model generates gain spectra as a function of carrier density. By matching peak modal gain obtained using the two approaches, reliable assessment of the carrier recombination coefficients can be made. At each injected carrier density, the current density can be written as

$$J = \frac{1}{\eta} [J_{\text{sp}} + qd(AN + CN^3)], \quad (4)$$

where η is the injection efficiency for the active region, which is defined as the DWELL layers. $J_{\text{sp}} = 2ed \int_{-\infty}^{\infty} d\omega S(\omega)$ is the

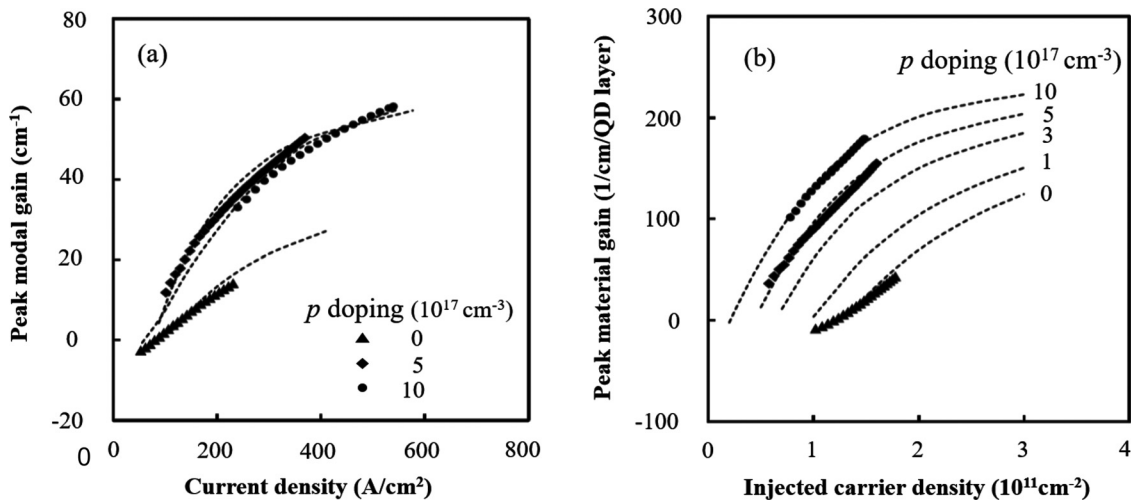


FIG. 3. (a) Peak modal gain versus current density. The points are from experiment. The curves are from calculated gain spectra such as shown in Fig. 2. Fitting and measured parameters for calculations are listed in Table I. (b) Peak material gain per QD layer versus injected carrier density. The curves are from the gain calculations. The curve fitting in (a) is used to extract the carrier density for each experimental data point. This allows the experimental data to be plotted in (b). All other parameters are the same as in Fig. 1.

TABLE I. Parameters from measurements and fitting to theory.

Parameter	Sample A	Sample B	Sample C
p -doping density N_p (cm ⁻³)	UID	5×10^{17}	1×10^{18}
QD density N_{QD} (cm ⁻²)	5×10^{10}	5×10^{10}	5×10^{10}
Confinement factor Γ	0.067	0.065	0.065
Injection efficiency η	85%	85%	85%
Internal loss α_i (cm ⁻¹)	7.9	7.9	7.9
Inh. broadening Δ_{inh} (meV)	10	10	10
Defect (SRH) loss coefficient A (s ⁻¹)	1.29×10^8	1.31×10^9	2.63×10^9
Auger coefficient C (cm ⁶ s ⁻¹)	1.71×10^{-26}	1.71×10^{-26}	1.85×10^{-26}

spontaneous emission current [factor 2 accounts for 2 TE polarizations in the QW plane, d is the thickness of the DWELL, and $S(\omega)$ is the spontaneous emission spectrum calculated from the gain model through detailed balance²⁷]. A and C are the fitting parameters related to the linear and cubic nonradiative recombination terms. They are commonly attributed to Shockley-Read-Hall (SRH) recombination and Auger recombination, respectively. The results of the fitting and other important device parameters from experiment are listed in Table I. The sensitivity of the extracted parameter to the measurement uncertainty has been discussed in a previous report.²⁶ Agreement between measured and calculated gain is depicted in Fig. 3. The differences between the shape of the gain curves when plotted against current density and injected carrier density speak volumes about the carrier recombination process introduced by p doping. As indicated in Table I, the Auger coefficient C remains relatively unchanged as doping density increases. This is consistent with the un-enhanced Auger recombination in the doped structure observed from PL²⁸ and ASE¹⁴ measurements. It is worth mentioning that the extracted C coefficient is larger compared to the previously reported value in InGaAs/GaAs QD laser.²⁹ A similar large C coefficient has been reported before in InGaN LEDs³⁰ and merits further investigation. The extracted SRH loss coefficient A , on the other hand, increases by 10 and 20 times compared to the UID case when doping density

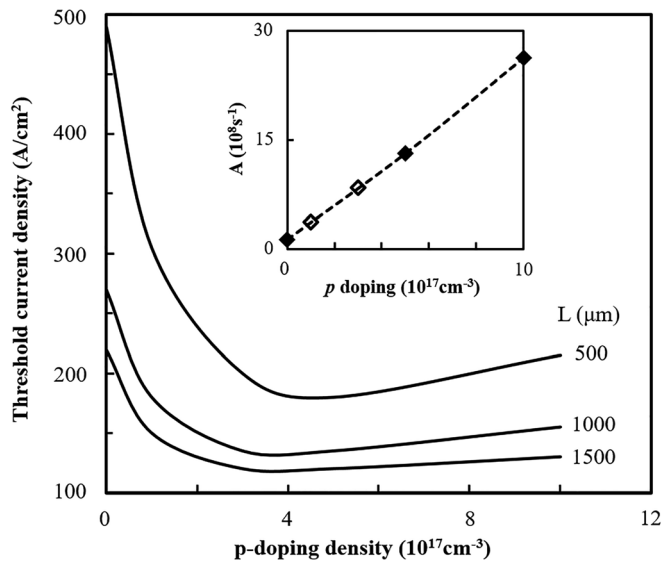


FIG. 4. Threshold current versus p -doping density for resonator lengths as labeled. The curves are obtained using Fig. 3(b) and the parameters in Table I. The lasers operate with 5 InAs QD layers, uncoated resonator facets, and a confinement factor of 0.065. The inset shows the dependence of SRH coefficient A on doping density.

reaches $5 \times 10^{17} \text{ cm}^{-3}$ and $1 \times 10^{18} \text{ cm}^{-3}$, suggesting increased defect levels at the mid bandgap. Due to the increased carrier loss at a doping level of $1 \times 10^{18} \text{ cm}^{-3}$, the added gain in the gain-carrier relationship [Fig. 3(b)] does not translate to a further improved gain-current relationship [Fig. 3(a)].

It is of more practical importance to discuss the overall effects of p doping on laser threshold. Based on calculated gain characteristics and extracted recombination coefficients in Table I, the dependence of threshold current density on the doping level is plotted in Fig. 4. Due to higher gain and lower transparency, as indicated in Fig. 3(b), the p -doped lasers are expected to show reduced threshold compared to the UID case. The laser threshold reaches minimum at around $5 \times 10^{17} \text{ cm}^{-3}$, above which the threshold starts to increase due to enhanced carrier recombination and gain saturation. As it has been pointed out, practical applications such as directly modulated lasers, mode-locked lasers, and narrow linewidth lasers require high differential gain (dG/dN). The increased slope in the gain-carrier curves, hence larger differential gain, at elevated doping densities depicted in Fig. 3(b) proves the advantage of having a modulation p -doped QD active region in these applications.

In summary, we have characterized the gain performance of QD lasers with varied modulation p -doping density through experiment and a first-principles gain model. The excess holes introduced by p doping enhance population inversion, which helps the laser reach higher gain and lower transparency current. On the other hand, the state-filling effect and the increased carrier scattering rate, reduce further increase in gain per for the same amount of additional dopant at higher doping density. p doping also creates increased SRH recombination, which starts to saturate the gain-current relationship above a certain doping concentration. Overall, the introduction of appropriate p doping density in the QD

active region will result in reduced threshold and increased differential gain, making QD lasers more competitive light sources for data communication, where energy efficiency, modulation speed, and spectra purity are crucial.

This research was supported by Advanced Research Projects Agency-Energy (ARPA-E) No. DE-AR000067 and the U.S. Department of Energy under Contract No. DE-AC04-94AL85000. We are thankful to M. J. Kennedy for device fabrication.

- ¹D. Thomson, A. Zilkie, J. E. Bowers, T. Komljenovic, G. T. Reed, L. Vivien, D. Marris-Morini, E. Cassan, L. Virot, J.-M. Fédéli *et al.*, *J. Opt.* **18**, 073003 (2016).
- ²A. Y. Liu, S. Srinivasan, J. Norman, A. C. Gossard, and J. E. Bowers, *Photonics Res.* **3**, B1 (2015).
- ³S. Chen, W. Li, J. Wu, Q. Jiang, M. Tang, S. Shutts, S. N. Elliott, A. Sobiesierski, A. J. Seeds, I. Ross *et al.*, *Nat. Photonics* **10**, 307 (2016).
- ⁴D. Jung, Z. Zhang, J. Norman, R. Herrick, M. Kennedy, P. Patel, K. Turnlund, C. Jan, A. Gossard, and J. E. Bowers, *ACS Photonics* **5**(3), 1094–1100 (2018).
- ⁵A. Y. Liu, R. W. Herrick, O. Ueda, P. M. Petroff, A. C. Gossard, and J. E. Bowers, *IEEE J. Sel. Top. Quantum Electron.* **21**, 690 (2015).
- ⁶D. Jung, R. Herrick, J. Norman, K. Turnlund, C. Jan, K. Feng, A. C. Gossard, and J. E. Bowers, *Appl. Phys. Lett.* **112**, 153507 (2018).
- ⁷Y. Wang, S. Chen, Y. Yu, L. Zhou, L. Liu, C. Yang, M. Liao, M. Tang, Z. Liu, J. Wu *et al.*, *Optica* **5**, 528 (2018).
- ⁸S. Liu, D. Jung, J. Norman, M. Kennedy, A. Gossard, and J. Bowers, *Electron. Lett.* **54**, 432 (2018).
- ⁹L. A. Coldren, S. W. Corzine, and M. L. Mashanovitch, *Diode Lasers and Photonic Integrated Circuits* (John Wiley & Sons, 2012), Vol. 218.
- ¹⁰D. J. Derickson, R. J. Helkey, A. Mar, J. R. Karin, J. G. Wasserbauer, and J. E. Bowers, *IEEE J. Quantum Electron.* **28**, 2186 (1992).
- ¹¹S. Melnik, G. Huyet, and A. V. Uskov, *Opt. Express* **14**, 2950 (2006).
- ¹²J. Tatebayashi, M. Nishioka, and Y. Arakawa, *Appl. Phys. Lett.* **78**, 3469 (2001).
- ¹³K. J. Vahala and C. Zah, *Appl. Phys. Lett.* **52**, 1945 (1988).
- ¹⁴P. M. Snowton, I. C. Sandall, H. Liu, and M. Hopkinson, *J. Appl. Phys.* **101**, 013107 (2007).
- ¹⁵V. Korenev, A. Savelyev, M. Maximov, F. Zubov, Y. M. Shernyakov, M. Kulagina, and A. Zhukov, *Appl. Phys. Lett.* **111**, 132103 (2017).
- ¹⁶O. Shchekin and D. Deppe, *Appl. Phys. Lett.* **80**, 2758 (2002).
- ¹⁷R. R. Alexander, D. T. Childs, H. Agarwal, K. M. Groom, H.-Y. Liu, M. Hopkinson, R. A. Hogg, M. Ishida, T. Yamamoto, M. Sugawara *et al.*, *IEEE J. Quantum Electron.* **43**, 1129 (2007).
- ¹⁸D. Inoue, D. Jung, J. Norman, Y. Wan, N. Nishiyama, S. Arai, A. C. Gossard, and J. E. Bowers, *Opt. Express* **26**, 7022 (2018).
- ¹⁹M. Maximov, Y. M. Shernyakov, F. Zubov, A. Zhukov, N. Y. Gordeev, V. Korenev, A. Savelyev, and D. Livshits, *Semicond. Sci. Technol.* **28**, 105016 (2013).
- ²⁰W. W. Chow, M. Lorke, and F. Jahnke, *IEEE J. Sel. Top. Quantum Electron.* **17**, 1349 (2011).
- ²¹D. T. Cassidy, *J. Appl. Phys.* **56**, 3096 (1984).
- ²²P. Andrekson, N. Olsson, T. Tanbun-Ek, R. Logan, D. Coblentz, and H. Temkin, *Electron. Lett.* **28**, 171 (1992).
- ²³D. A. Ackerman, G. E. Shtengel, M. S. Hybertsen, P. A. Morton, R. F. Kazarinov, T. Tanbun-Ek, and R. Logan, *IEEE J. Sel. Top. Quantum Electron.* **1**, 250 (1995).
- ²⁴W. W. Chow and F. Jahnke, *Prog. Quantum Electron.* **37**, 109 (2013).
- ²⁵See <http://www.nextnano.com/nextnano3/> for “Nextnano³” (accessed 2018-04-18).
- ²⁶W. W. Chow, A. Y. Liu, A. C. Gossard, and J. E. Bowers, *Appl. Phys. Lett.* **107**, 171106 (2015).
- ²⁷C. Henry, R. Logan, and F. Merritt, *J. Appl. Phys.* **51**, 3042 (1980).
- ²⁸T. Badcock, R. Royce, D. Mowbray, M. Skolnick, H. Liu, M. Hopkinson, K. Groom, and Q. Jiang, *Appl. Phys. Lett.* **90**, 111102 (2007).
- ²⁹S. Ghosh, P. Bhattacharya, E. Stoner, J. Singh, H. Jiang, S. Nuttinck, and J. Laskar, *Appl. Phys. Lett.* **79**, 722 (2001).
- ³⁰H.-Y. Ryu, H.-S. Kim, and J.-I. Shim, *Appl. Phys. Lett.* **95**, 081114 (2009).